GEOPHYSICS, VOL. 62, NO. 3 (MAY-JUNE 1997); P. 895—905, 14 FIGS., 2 TABLES.

Seismic attenuation tomography using the frequency shift method

Youli Quan* and Jerry M. Harris†

ABSTRACT

We present a method for estimating seismic attenuation based on frequency shift data. In most natural materials, seismic attenuation increases with frequency. The high-frequency components of the seismic signal are attenuated more rapidly than the low-frequency components as waves propagate. As a result, the centroid of the signal's spectrum experiences a downshift during propagation. Under the assumption of a frequency-independent Q model, this downshift is proportional to a path integral through the attenuation distribution and can be used as observed data to reconstruct the attenuation distribution tomographically. The frequency shift method is applicable in any seismic survey geometry where the signal bandwidth is broad enough and the attenuation is high enough to cause noticeable losses of high frequencies during propagation. In comparison to some other methods of estimating attenuation, our frequency shift method is relatively insensitive to geometric spreading, reflection and transmission effects, source and receiver coupling and radiation patterns, and instrument responses. Tests of crosswell attenuation tomography on 1-D and 2-D geological structures are presented.

INTRODUCTION

Recent improvements of seismic data quality, especially crosswell data, make it possible to estimate the heterogeneous distribution of seismic attenuation from the dispersion of amplitude with frequency. It has long been believed that attenuation is important for the characterization of rock and fluid properties, e.g., saturation, porosity, permeability, and viscosity, because attenuation is more sensitive than velocity to some of these properties (e.g., Best et al., 1994). Measurements of both velocity and attenuation provide complementary information about rock properties. Attempts at estimating attenuation tomographically have persisted for years. For example, Brzostowski and McMechan (1992), and Leggett et al. (1992) used the change in seismic amplitude as observed data for attenuation tomography. However, amplitudes are easily contaminated by many factors such as scattering, geometric spreading, source and receiver coupling, radiation patterns, and transmission/reflection effects. Therefore, it is often difficult to obtain reliable attenuation estimates from the amplitude decay method. Here we use a method based on pulse broadening. As a seismic pulse propagates in a medium, the shape of the pulse broadens because of dispersion caused by attenuation. The rise time associated with this broadening effect has been used to estimate attenuation (e.g., Kjartansson, 1979; Zucca, et al., 1994). However, a precise and robust measurement of the rise time is difficult for field data; therefore, we use a related quantity, the estimated shift in the centroid of the pulse spectrum. To first order, the frequency shift or pulse broadening for wave packets is not affected by far-field geometrical spreading and transmission/reflection losses. Therefore, the measurement based on frequency shifts appears to be more reliable than the amplitude decay method. It should be pointed out that the frequency shift method, in fact, measures the pulse broadening in frequency domain, and the rise-time method measures a pulse broadening in time domain. The measurement in frequency domain may be more convenient and stable.

Seismic wave attenuation includes intrinsic attenuation and scattering attenuation. Both of them can cause wave dispersion. Scattering transfers wave energy to later arrivals or to other directions. Scattering attenuation depends on the scale of heterogeneites. When the scale of heterogeneities is much smaller than the characteristic wavelength, the high-frequency components are lost because of destructive interference (Marion and Coudin, 1992). Intrinsic attenuation transfers wave energy to heat. In this study, we concentrate on the intrinsic attenuation and try to reduce the influence of the scattering attenuation. In the situation when the scattering attenuation

Presented at the 63rd Annual International Meeting, Society of Exploration Geophysicists. Manuscript received by the Editor November 15, 1995; revised manuscript received August 29, 1996.
*Formerly Department of Geophysics, Stanford University, Stanford, California 94305-2215; presently Texaco EPTD, 3901 Briarpark, Houston, TX 77042.
†Department of Geophysics, Stanford University, Stanford, California 94305-2215.

cannot be ignored, the estimated attenuation is a combination of intrinsic and scattering effects.

Experiments indicate that the intrinsic attenuation for many rocks is proportional to frequency (e.g., Johnston, 1981). The high-frequency components of an incident wave are more attenuated during wave propagation than the low-frequency components. If we examine the shape of the frequency spectrum, we find that its centroid experiences a downshift in frequency as the wave propagates, since the high-frequency part of the spectrum decreases faster than the low-frequency part. This phenomenon has been observed in vertical seismic profiling data (Hauge, 1981). In this paper, we propose an approach to estimate the attenuation distribution in an inhomogeneous medium based on this frequency shift. Since we want a quantitative estimate of the attenuation, we need to derive a relationship that links the frequency shift to the attenuation parameters describing the medium. We use a method that is similar to the approach proposed in Dines and Kak (1979), and later used by Parker et al. (1988) for medical attenuation tomography. This method requires the data be broad band so that the frequency shift can be estimated easily. High-frequency crosswell surveys provide good examples of such data.

In this paper, we present the basic theory of the frequency shift method and discuss how the frequency shift is related to the attenuation coefficient for various signal spectra. We then test the frequency shift method in crosswell attenuation tomography for both synthetic and field data.

THEORY

The attenuation model

For the purpose of estimating attenuation, we assume that the process of wave propagation is described by linear system theory. If the amplitude spectrum of an incident wave is $S(f)$ and the instrument/medium response is $G(f)H(f)$, then the received amplitude spectrum $R(f)$ may be, in general, expressed as (see Figure 1)

$$R(f) = G(f)H(f)S(f), \tag{1}$$

where the factor $G(f)$ includes geometrical spreading, instrument response, source/receiver coupling, radiation patterns, and reflection/transmission coefficients, and the phase accumulation caused by propagation, and $H(f)$ describes the attenuation effect on the amplitude. In this study we concentrate on the absorption property of the medium; therefore we call $H(f)$ the attenuation filter. Experiments indicate the attenuation is usually proportional to frequency, that is, response $H(f)$ may be expressed (Ward and Toksöz, 1971) as

$$H(f) = \exp\left(-f \int_{ray} \alpha_o \, d\ell\right), \tag{2}$$

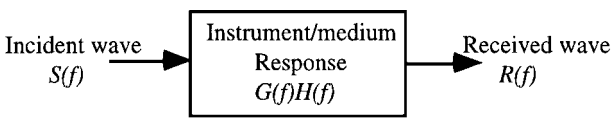

FIG. 1. Linear system model for attenuation.

where the integral is taken along the raypath, and α_o is attenuation coefficient defined by

$$\alpha_o = \frac{\pi}{Qv}, \tag{3}$$

i.e., attenuation is linearly proportional to frequency, where Q is medium's quality factor and v is wave velocity. Note that our attenuation factor α_o is different from the usually defined attenuation coefficient $\alpha = \alpha_o f$. This linear frequency model is useful in demonstrating the frequency shift method. More complex models, for example, $\alpha = \alpha_o f^p$ with $p \neq 1$, can be considered in a similar way (Narayana and Ophir, 1983).

Our goal is to estimate the medium response $H(f)$, or more specifically, the attenuation coefficient α_o, from knowledge of the input spectrum $S(f)$ and the output spectrum $R(f)$. A direct approach is to solve equation (1) by taking the logarithm and obtaining

$$\int_{ray} \alpha_o \, d\ell = \frac{1}{f} \ln\left[\frac{GS(f)}{R(f)}\right]. \tag{4}$$

Equation (4) may be used to estimate the integrated attenuation at each frequency and is called the amplitude decay method. However, as described above, the factor G lumps many complicated processes together, and is very difficult to determine. Furthermore, the calculation of attenuation based on individual frequencies is not robust because of poor individual signal-to-noise. To overcome some of these difficulties, we can rewrite equation (4) as

$$Y(f) = Cf + B \tag{5}$$

where, $Y(f) = \ln[S(f)/R(f)]$, $C = \int_{ray} \alpha_o \, d\ell$, and $B = -\ln(G)$. It can be seen from equation (5) that the integrated attenuation C is the slope of the plot of $Y(f)$ versus frequency f. The attenuation estimation based on equation (5) uses the spectral ratio, $S(f)/R(f)$, over a range of frequencies, and is called the spectral ratio method. This method may remove the effect of factor G, when G does not depend on frequency f. In the following, we propose a statistics-based method that estimates the attenuation coefficient α_o from the spectral centroid downshift over a range of frequencies.

Spectral centroid and variance

We define the centroid frequency of the input signal $S(f)$ as

$$f_S = \frac{\int_0^\infty f S(f)\, df}{\int_0^\infty S(f)\, df}, \tag{6}$$

and the variance to be

$$\sigma_S^2 = \frac{\int_0^\infty (f - f_S)^2 S(f)\, df}{\int_0^\infty S(f)\, df}. \tag{7}$$

Similarly, the centroid frequency of the received signal $R(f)$ is

$$f_R = \frac{\int_0^\infty f R(f)\, df}{\int_0^\infty R(f)\, df}, \tag{8}$$

and its variance is

$$\sigma_R^2 = \frac{\int_0^\infty (f - f_R)^2 R(f)\, df}{\int_0^\infty R(f)\, df}, \tag{9}$$

where $R(f)$ is given by equation (1). If we take the factor G to be independent of frequency f, f_R and σ_R^2 will be independent of G. This is a major advantage of using the spectral centroid and variance rather than the actual amplitudes.

Let us consider a special case where the incident spectrum $S(f)$ is Gaussian, i.e., given by the equation

$$S(f) = \exp\left[-\frac{(f - f_o)^2}{2\sigma_S^2}\right]. \tag{10}$$

The source and receiver centroid frequencies are (see Appendix)

$$f_S = f_o, \tag{11a}$$

and

$$f_R = f_S - \sigma_S^2 \int_{ray} \alpha_o \, d\ell, \tag{11b}$$

respectively. We can rewrite equation (11b) as a line integral suitable for tomographic inversion as

$$\int_{ray} \alpha_o \, d\ell = (f_S - f_R)/\sigma_S^2. \tag{12}$$

Figure 2 gives a pictorial description for the Gaussian spectra. Using the values of f_S, f_R, and σ_S^2 given with Figure 2, we get the inversion result to exactly match the value, $\int \alpha_o \, d\ell = 0.0008$, used in computing the filter $H(f)$ for this example. Here, the factor G in equation (1) is assumed to be 1.

A similar derivation (see Appendix) for non-Gaussian spectra (boxcar and triangular) leads to the following results. Numerical results for these special case spectra are summarized in Table 1. For the boxcar spectrum with bandwidth B, we obtain an approximate formula

$$\int \alpha_o \, d\ell \approx 12(f_S - f_R)/B^2, \qquad B \int \alpha_o \, d\ell \ll 1. \tag{13}$$

Figure 3 gives a pictorial description of frequency shift for the boxcar spectrum. Plugging the values of f_S, f_R, and B shown in Figure 3 into equation (13), we obtain the inversion result $\int \alpha_o \, d\ell = 0.000797$ which is very close to the given value of 0.0008. For a triangular spectrum with bandwidth B, we obtain another approximate formula

$$\int \alpha_o \, d\ell \approx 18(f_S - f_R)/B^2, \qquad B \int \alpha_o \, d\ell \ll 1. \tag{14}$$

Under the assumption of a constant Q model we have derived tomographic equations (12), (13), and (14) for Gaussian, rectangular and triangular spectra, respectively. These equations show that the attenuation coefficient for an inhomogeneous medium $\alpha_o(x, z)$ can be obtained by measuring the centroid frequency downshift $(f_S - f_R)$ between the incident and transmitted signals. The integrated attenuation equals this frequency downshift multiplied by a scaling factor. From equations (12–14), we find that a broader input bandwidth (larger σ_S or B) leads to a larger frequency change. Therefore, a broad input frequency band is important for a robust estimation of $\alpha_o(x, z)$. Crosswell seismic profiling with a high-frequency downhole source provides a good opportunity to test attenuation tomography using this frequency shift method.

The tomographic formula relating frequency shift with the attenuation projection is exact only for Gaussian spectra, i.e., equation (12). Nevertheless, the approximate formulas, equations (13) and (14), are useful in practical situations where Gaussian spectra can not be assumed. Although equations (12), (13), and (14) are derived from spectra of different shapes, they are somewhat similar. This similarity implies the robustness of this method, that is, the estimate of relative attenuation is not sensitive to a small change in spectrum shapes.

Table 1. Numerical results for three special spectra.

Spectrum Shape	Model $\int \alpha_o \, d\ell$	Estimated $\int \alpha_o \, d\ell$	f_S (Hz)	σ_S^2 or B^2 (Hz^2)	f_R (Hz)	σ_R^2 or B^2 (Hz^2)
Gaussian	0.0008	0.0008	400	12730	389.8	12730
Boxcar	0.0008	0.000797	400	800^2	357.5	800^2
Triangular	0.0008	0.000765	266.3	800^2	239.1	800^2

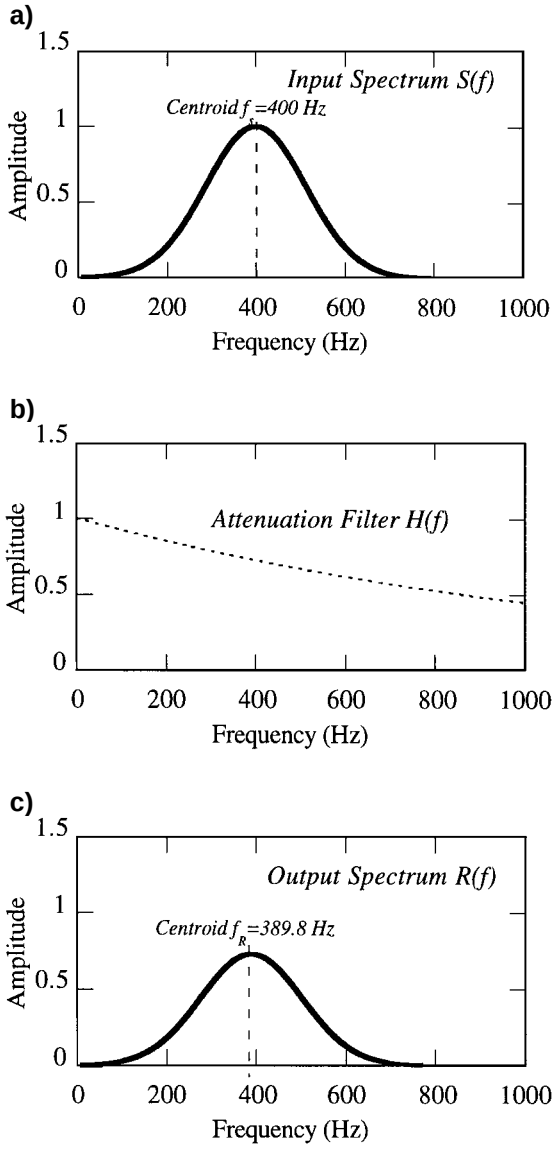

FIG. 2. (a) An input spectrum of Gaussian shape with center frequency (spectral centroid) of 400 Hz and variance of 12, 730 Hz^2. (b) Medium response for $\int \alpha_o \, d\ell = 0.0008$. (c) The output spectrum remains Gaussian shape with a variance of 12, 730 Hz^2, but the spectral centroid is shifted to 389.8 Hz.

PRACTICAL CONSIDERATIONS

Static correction of source frequency

Equation (12) is the basic formula for attenuation tomography. It can be written in a discrete form as

$$\sum_j \alpha_{oj}^i \ell_j^i = \frac{f_S - f_R^i}{\sigma_S^2}. \tag{15}$$

Here the index i represents the ith ray, j the jth parameterized pixel of the medium, and ℓ_j^i is the length of ith ray within the jth pixel. In practice, we can measure f_R from recorded seismograms, but may not directly measure the source centroid frequency f_S and its variance σ_S^2. For the constant Q-model described by equation (2) and Gaussian spectrum given by equation (10), the source spectrum $S(f)$ and receiver spectrum $R(f)$ exhibit the same variance σ_S^2. Therefore, we may choose the average of σ_R^2 at the receivers as the estimate of the source variance σ_S^2. While the centroid frequency f_S of the incident wave may also be unknown, we include it along with the matrix of unknown attenuation values. We then simultaneously invert for both the attenuation coefficients α_j^i and the source frequency f_S as follows. Let

$$f_S = \bar{f}_S + \Delta f, \tag{16}$$

where $\bar{f}_S = \max\{f_R^i\}$ is an initial estimation of f_S, and Δf is a correction to be found. Then

$$\frac{f_S - f_R^i}{\sigma_S^2} = \frac{\bar{f}_S + \Delta f - f_R^i}{\sigma_S^2} = \frac{\bar{f}_S - f_R^i}{\sigma_S^2} + \frac{\Delta f}{\sigma_S^2}. \tag{17}$$

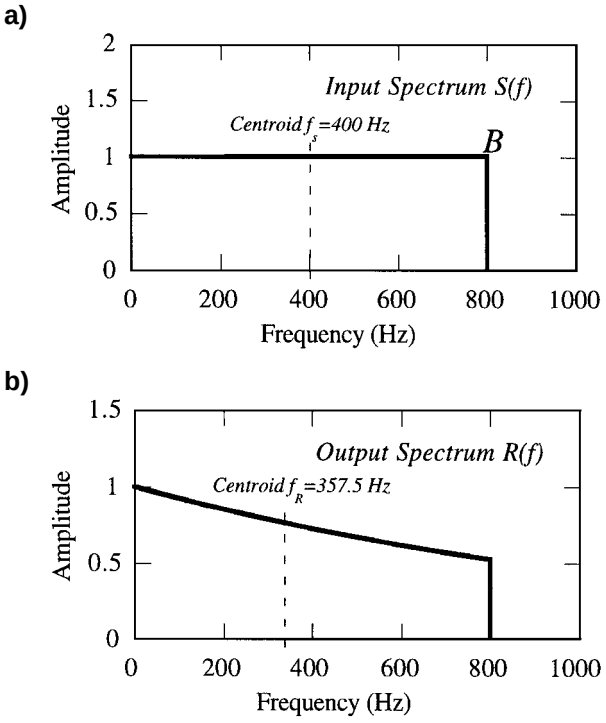

FIG. 3. (a) A boxcar input spectrum with spectral centroid of 400 Hz and band width is 800 Hz. (b) The spectral centroid of the output spectrum shifts to 357.5 Hz. The medium response is same as Figure 2b.

Equation (15) can now be written as

$$\sum_j \alpha_j^i \ell_j^i - \frac{\Delta f}{\sigma_S^2} = \frac{\bar{f}_S - f_R^i}{\sigma_S^2}, \tag{18}$$

where α_j^i and Δf are the unknowns to be determined.

Data processing

The main purpose of data processing is to extract the direct wave and reduce the interference caused by scattering. To do this we first pick and align the direct wave. Next we mix traces to reduce interference caused by scattering, and perform a fast Fourier transform (FFT) on the direct arrival isolated by a short time window. The centroid frequency f_R and variance σ_S^2 are then calculated by equations (8) and (9). If we treat $(\bar{f}_S - f_R^i)/\sigma_S^2$ as "data," α_j^i as "unknown," and then add one more term $-\Delta f/\sigma_S^2$ into the system, then we only need to modify slightly the algorithms and programs used for traveltime tomography to do the attenuation tomography.

In most situations, the medium is heterogeneous in both velocity and attenuation. Our procedure is to use the traveltimes first to estimate the velocity distribution and the ray paths, then use the frequency shift data and these raypaths to estimate attenuation. Finally, because the Q model underlies the development of the theory, we estimate the Q distribution by combining the velocity and attenuation tomograms. However, the image of the attenuation factor can be used as the final result.

NUMERICAL TESTS

VSP geometry: An ideal test

Let us first examine the validity of equation (12) by considering an ideal synthetic example in the zero offset vertical seismic profiling (VSP) geometry. For this geometry, both input and output centroid frequencies f_S and f_R are measurable since signals in two successive receivers can be viewed as the incident and transmitted spectra. In this case, we may write equation (12) as

$$\alpha_{oi} = \frac{1}{\sigma_i^2}\frac{\Delta f_i}{\Delta z_i}, \tag{19}$$

where $\Delta f_i = f_i - f_{i+1}$ is the centroid frequency difference between two successive depth levels, Δz_i is the distance between these two receivers, α_{oi} is the average attenuation coefficient between the two levels, and σ_i^2 the variance at ith receiver.

The generalized reflection and transmission coefficients method (e.g., Luco and Apsel, 1983; Chen et al., 1996) is used to calculate the complete wavefield in layered media. The attenuation is introduced through the complex velocity defined by

$$v(f) = v(f_{ref})\left[1 + \frac{1}{\pi Q}\log\left(\frac{f}{f_{ref}}\right) - \frac{i}{2Q}\right], \tag{20}$$

where Q is the quality factor for either P-waves or S-waves, and v is either the P-wave velocity or S-wave velocity. A vertical seismic profile is calculated at 220 receivers for a source located at the surface. Figures 4a and 4b show the P-wave velocity and Q-value parameters of this model. The frequency band of the source is 10 Hz–2010 Hz. This frequency band is much broader than the real vertical seismic profiling,

but it is used here to illustrate the range of typical crosswell data for which this algorithm was developed initially.

We select a time window that isolates the first arrival. Figure 4c is a plot of the centroid frequency estimated from the synthetic data. The centroid frequency decreases from 370 Hz to 280 Hz over a depth range of 1000 ft (305 m). After smoothing the frequency shift data and applying equation (19), we obtain an estimate of the attenuation coefficient α_o. Then using the definition $Q = \pi/(\alpha_o v)$, we get the estimated Q-values shown in Figure 5a. The reconstructed Q-value (dotted line), fits the original model (solid line) quite well. The deviations of the inversion result near interfaces are caused by the interference of reflections in the estimation of the frequency shift near interfaces. Therefore, the thicker the layer, the better the

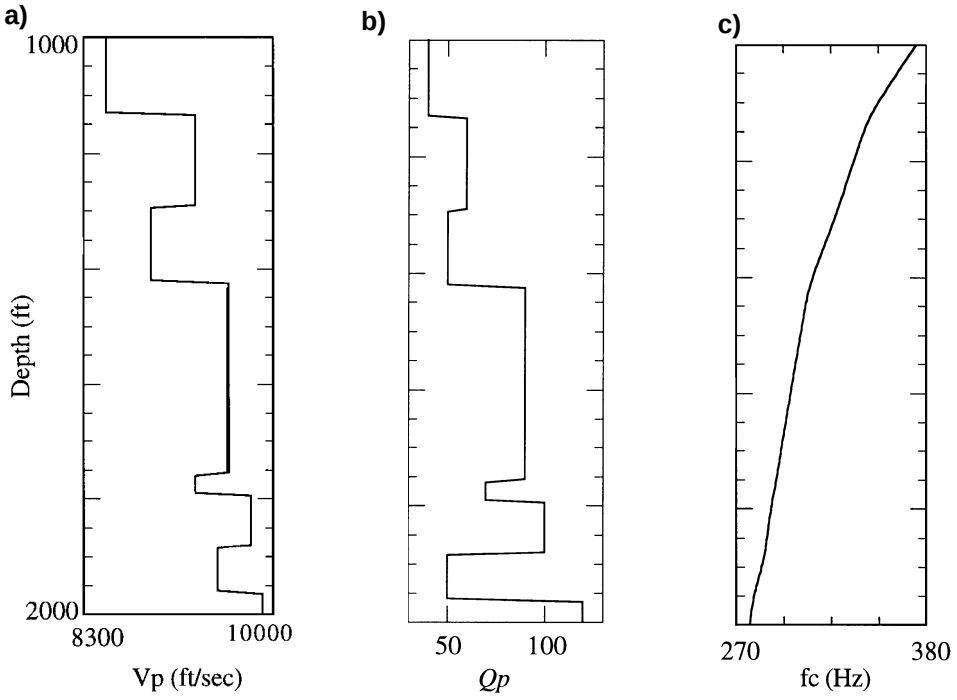

FIG. 4. The velocity and Q-value shown in (a) and (b) are used to calculate a zero offset VSP, and (c) is a plot of the centroid frequency corresponding to the direct wave in this VSP.

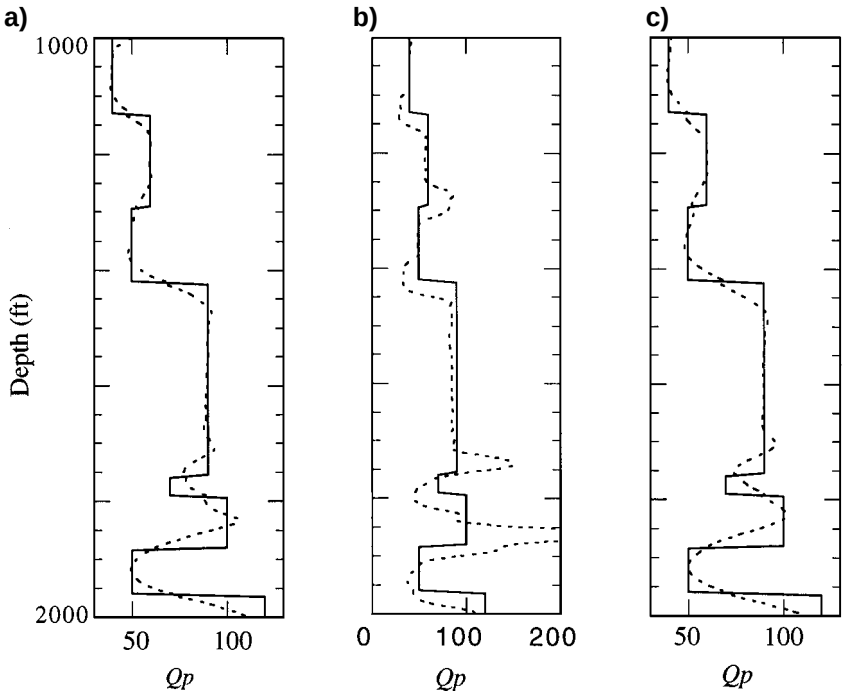

FIG. 5. Reconstructed Q-values (dotted lines) using the frequency shift method (a), the amplitude decay method (b), and the spectral ratio method (c).

inversion result. However, even for a relatively thin layer, the layer around the depth of 1770 ft (540 m), we still obtain a satisfactory result. We also apply the amplitude decay method [equation (4)] and the spectral ratio method [equation (5)] to the same synthetic data. Figure 5b shows the results using the amplitude decay method for peak frequencies. The reconstruction is poor, especially near the interfaces. Figure 5c is Q-value reconstruction using the spectral ratio method. It can been seen from Figures 5a and 5c that the reconstructed Q-value by the spectral ratio method is similar to the frequency shift method. Both of them fit the original model quite well. Since the frequency shift method is based on the statistics of the spectrum, it may be more robust than the spectral ratio method. The spectral ratio method requires a complete spectrum as reference for the calculation of ratio. In many cases, this reference spectrum is not available. For the frequency shift method, we only need a reference frequency. This feature makes the frequency shift method very suitable for attenuation tomography.

The source signature used in this example is a Ricker wavelet (not the Gaussian assumed in theory). Figure 6 shows the received spectrum at a depth of 1575 ft (480 m). For the frequency shift method, the centroid frequency and the variance are calculated using equations (8) and (9), respectively. Then, equation (19) is used for the attenuation estimation. Though equation (19) is derived from the spectrum with Gaussian shape, it still gives a good result for the Ricker wavelet. Thus, it appears from this synthetic test that equation (19) can also be used for other spectra, if the Gaussian is an approximate fit to them. Reflections near interfaces are a major noise source in this test. To reduce reflections, we use a model that has a constant velocity distribution but with the same Q-value distribution as in Figure 4b. For this model, the frequency shift method, the spectral ratio method, and the amplitude decay method give the same reconstruction results shown in Figure 7.

Crosswell seismic profiling

For our first synthetic crosswell tomographic simulation, we use a simple 1-D model shown in Figure 8a. We place 51 sources and 51 receivers with an offset of 400 ft (120 m). Figures 8b and 8c give a common-source gather in time domain and frequency domain, respectively. Figure 9 is the reconstruction of Q-values. The second synthetic example has two abnormal structures that terminate between wells. Figure 10a gives the original model. Again we place 51 sources in a well and 51 receivers in the formation. Both source interval and receiver interval are 2 ft. A Ricker wavelet with a peak frequency of 1000 Hz is used as the source signature. Figure 10b shows the inversion result. The reconstructed Q-values in Figures 9 and 10b are both quite close to the given ones. The tomography, based on the line integral defined by equation (12), is capable of imaging the Q field very well.

In the frequency shift method, information on wave dispersion is used to estimate attenuation. Therefore, the grid dispersion in the numerical methods would introduce serious numerical error in the forward modeling. For the model shown in Figure 10a, we used a semi-analytical method (Quan et al., 1996) for the calculation of synthetic seismograms. There is no grid dispersion in the computing. This modeling method simulates the complete viscoelastic wavefield in media with complex structures. The model also includes a source borehole.

To perform the attenuation tomography, we first need calculate the raypath. The error in the velocity estimation can affect the raypath, and therefore the attenuation estimation result. Figure 11 shows a synthetic example to investigate how the velocity error influences the attenuation tomography using the frequency shift method. We use a two-layer model with velocities $V_1 = 4$ km/s and $V_2 = 3$ km/s. In Test I, we set $V_1 = 3.5$ km, $V_2 = 3$ km/s and perform inversion. In Test II, we

Table 2. Effects of velocity error on the attenuation tomography.

	V_1 (km/s)	V_2 (km/s)	Q_1	Q_2
Given model	4	3	80	50
Test I	3.5	3	94	52
Test II	3.5	3.5	155	44

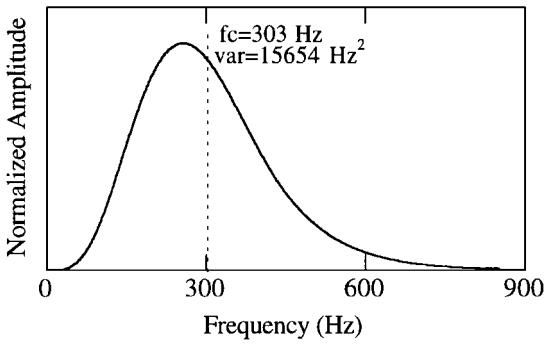

FIG. 6. The spectrum at depth 1575 ft. This is a Ricker wavelet in frequency domain. With the calculated centroid and variance, we use a Gaussian shape to fit this curve.

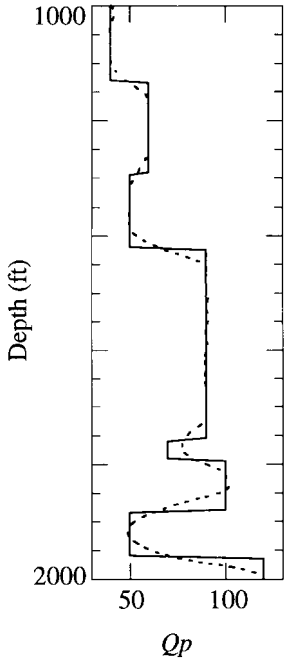

FIG. 7. The reconstructed Q-values (dotted line) for a model that has a constant velocity distribution.

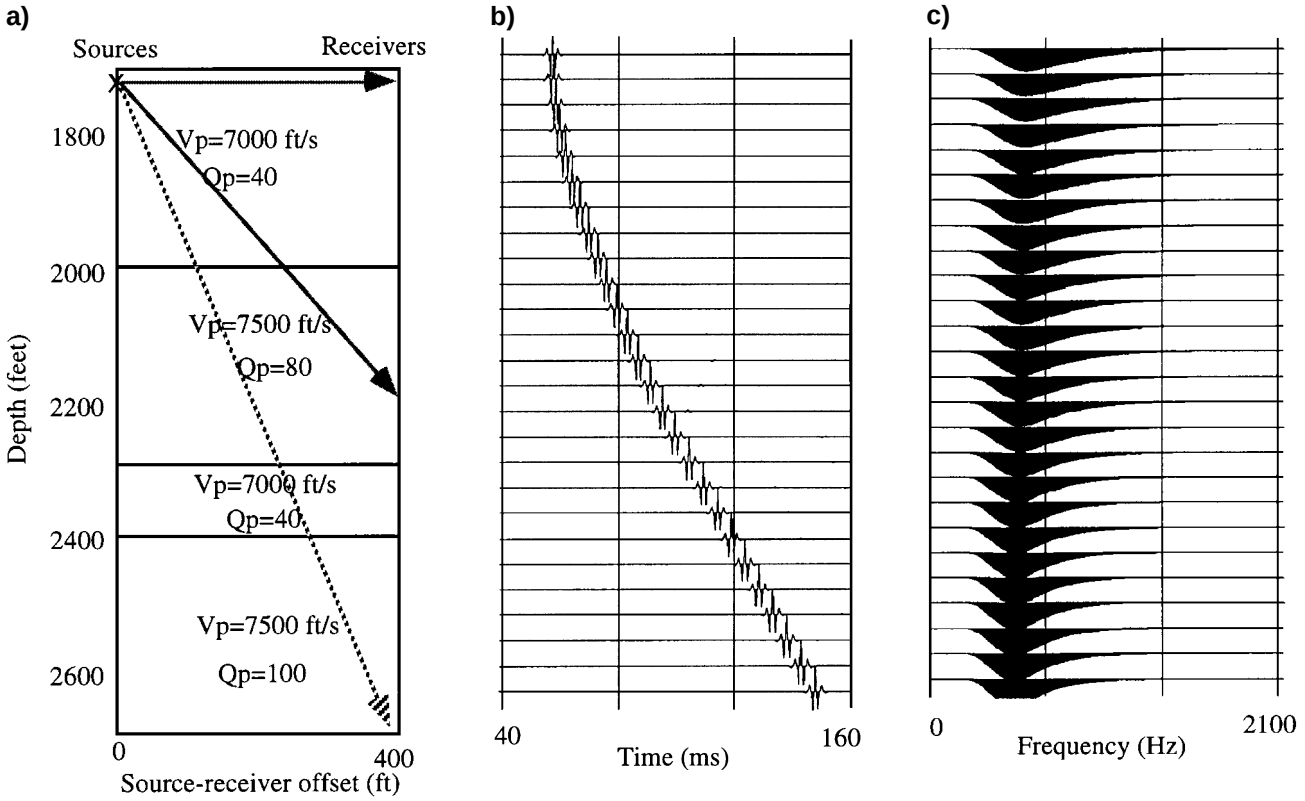

FIG. 8. The synthetic forward modeling for crosswell attenuation tomography. A layered model (a) for crosswell profiling is calculated. A point source with Ricker wavelet is used. We show a common-source gather in time and frequency domains in (b) and (c), respectively. The spectral downshift can be seen in (c).

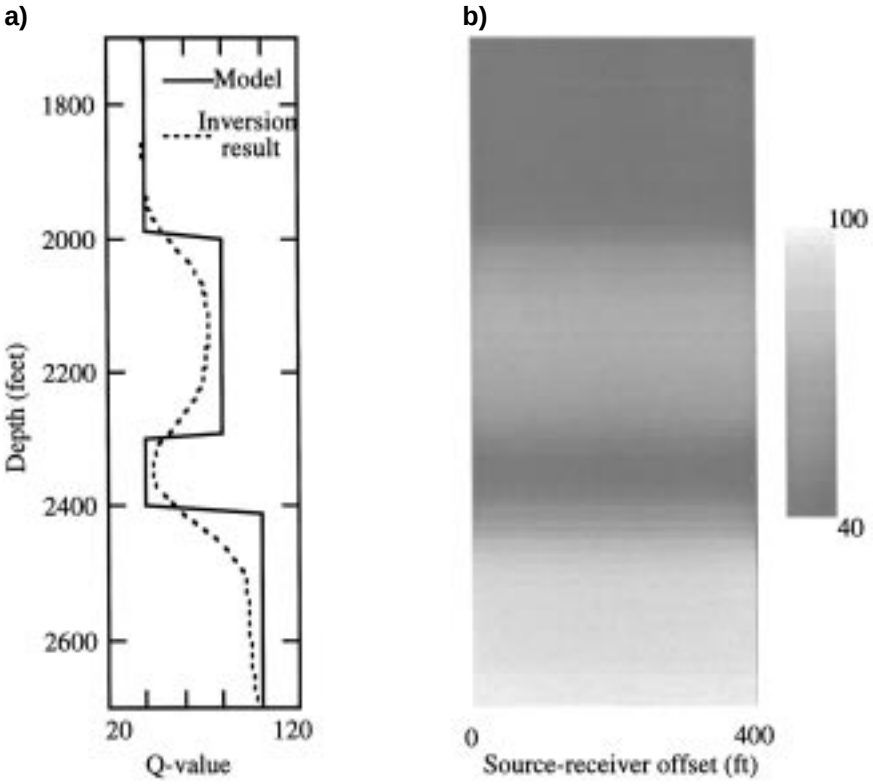

FIG. 9. The tomographic inversion result of the synthetic test. The dotted line in (a) is the profile of the 1-D imaging (b). The comparison in (a) shows the inversion is pretty close to the given model.

set $V_1 = 3.5$ km/s, $V_2 = 3.5$ km/s and perform inversion. The testing results are shown in Table 2. For this particular model, if we use straight raypaths (Test II) instead of true raypaths, the estimated Q-values are 155 and 44, corresponding to the given values 80 and 50, respectively. The error in velocity estimation exhibits a significant effect on the attenuation tomography. Bending rays and good velocity estimation are important.

APPLICATIONS TO FIELD DATA

One-dimensional geological structure

For field data, we first choose a data set collected at BP's Devine test site where the lithology is layer cake and approximately one dimensional. A linear sweep from 200 Hz to 2000 Hz was used as the source spectrum. Figure 12 shows the traveltime and centroid frequency picks from this field data set. It can be seen from these picks that the high centroid frequency correlates to the low traveltime. This correlation indicates that the high velocity formation in this area has low attenuation. We first use traveltime tomography to reconstruct the velocity structure and obtain raypaths. Then, we use the raypaths and centroid frequencies to reconstruct the attenuation structure. A 1-D model is assumed for this inversion problem. Figure 13 shows the velocity and attenuation reconstructions. For the attenuation tomography, the starting modeling is a homogeneous model that is calculated using the average centroid frequency shift. The initial source frequency $\bar{f}_S$ is 1750 Hz. After inversion, the final source frequency f_S is found to be 1520 Hz. The attenuation coefficient α_o and velocity v are converted to Q-values using equation (3). The lithology and the sonic log are also shown in Figure 13 for comparison. They exhibit an excellent geometric agreement with the inversion results. As we expect, Figure 13 shows that shales and sands exhibit lower Q-value and slower velocity, and that limestone has higher Q-value and faster velocity.

2-D geological structure

The second crosswell data set was collected from a reef structure in West Texas. This geological structure is strongly two-dimensional and is complicated. Only the source well penetrated the carbonate reef target. The starting model for inversion is homogeneous. The centroid frequency picks of this data range from 600 Hz to 1000 Hz. The maximum frequency 1000 Hz is chosen as the initial source frequency $\bar{f}_S$. The final source frequency f_S is found to be 850 Hz. Figure 14 shows the 2-D P-wave velocity and attenuation tomograms that reveal a consistent image of the lateral variations of the carbonate reef buildup.

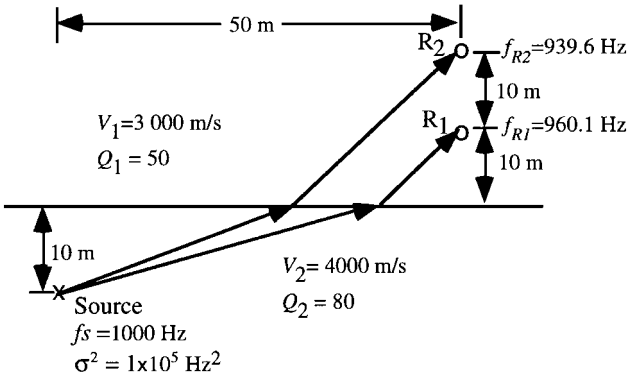

FIG. 11. This is an example showing the effect of the error in velocity estimation on the attenuation tomography. There are two layers, one source and two receivers in the model. Using the given model parameters, we calculate the centroid frequencies at receivers. For the inversion, if we use the correct (given) velocities, the Q-values for two layers are recovered correctly. If we add some errors to V_1 and/or V_2 and perform inversion, the recovered Q-values also have errors. Table 2 gives the results of two such tests.

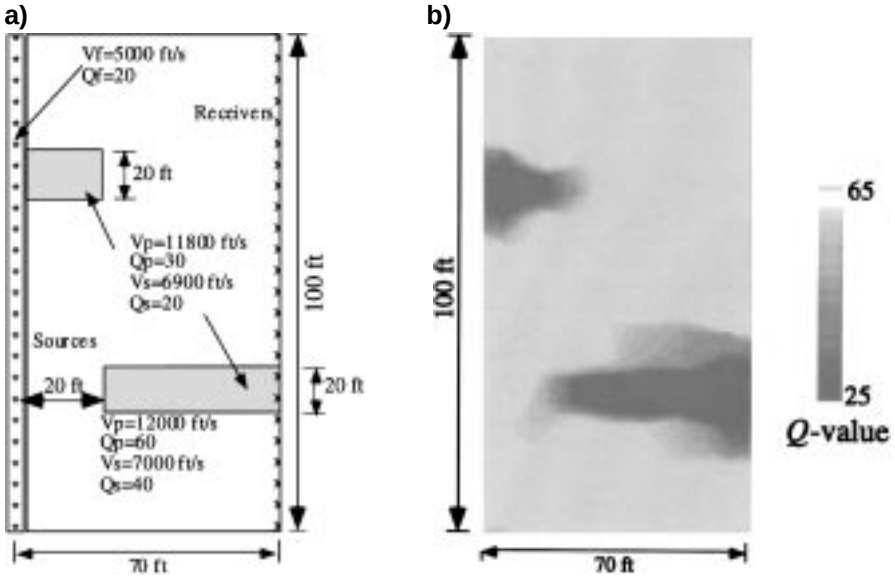

FIG. 10. A synthetic test on 2-D attenuation tomography. (a) is the original model. There are two low Q-value areas in this model, and (b) is the reconstructed Q-value distribution.

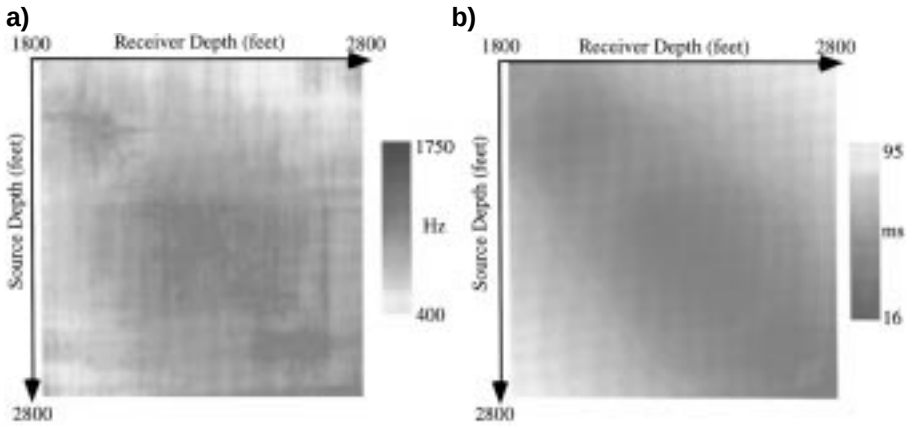

FIG. 12. The data picked from the Devine survey for the attenuation tomography. The traveltime of the direct *P*-wave is shown in (b), which is used to obtain a velocity model and raypaths. With these raypaths and the *P*-wave centroid frequency shown in (a) we can perform the attenuation tomography. A horizontal line in (a) or (b) represents a common source gather and a vertical line represents a common receiver gather. From these picks we can see a good correlation between traveltime and centroid frequency. The high frequency (dark color) corresponds to the high *Q*-value formation and correlates to the low traveltime (dark color) that corresponds to the high velocity formation.

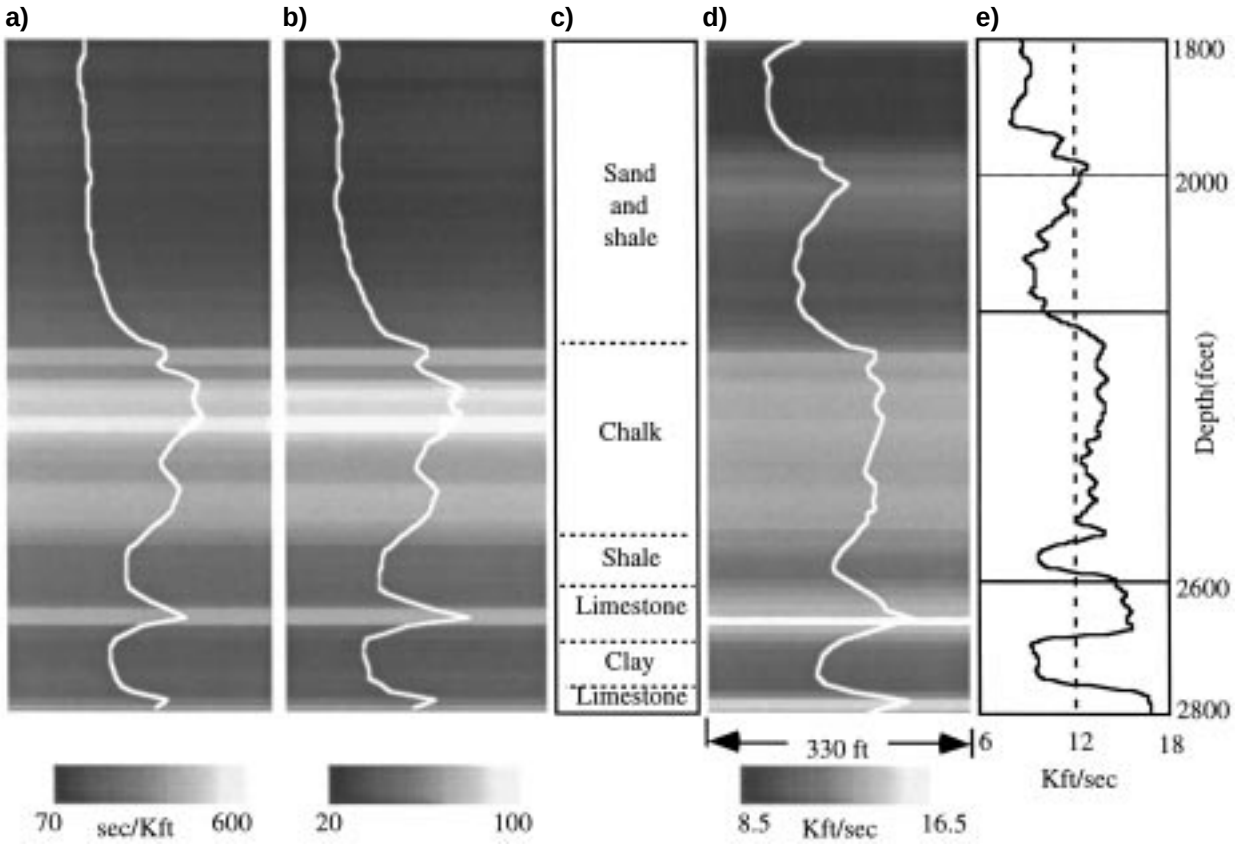

FIG. 13. Attenuation and velocity tomography for the Devine survey. (a) Crosswell $1/\alpha_o$; (b) Crosswell $Q(=\pi/v\alpha_o)$; (c) Lithology; (d) Crosswell velocity; (e) Sonic log velocity. We first calculate the velocity (v) and attenuation coefficient (α_o), then convert them to *Q*-value. To make a closer comparison, we plot the profile curves within the tomograms. It can be seen that *Q*-value, velocities and lithology exhibit a good correlation.

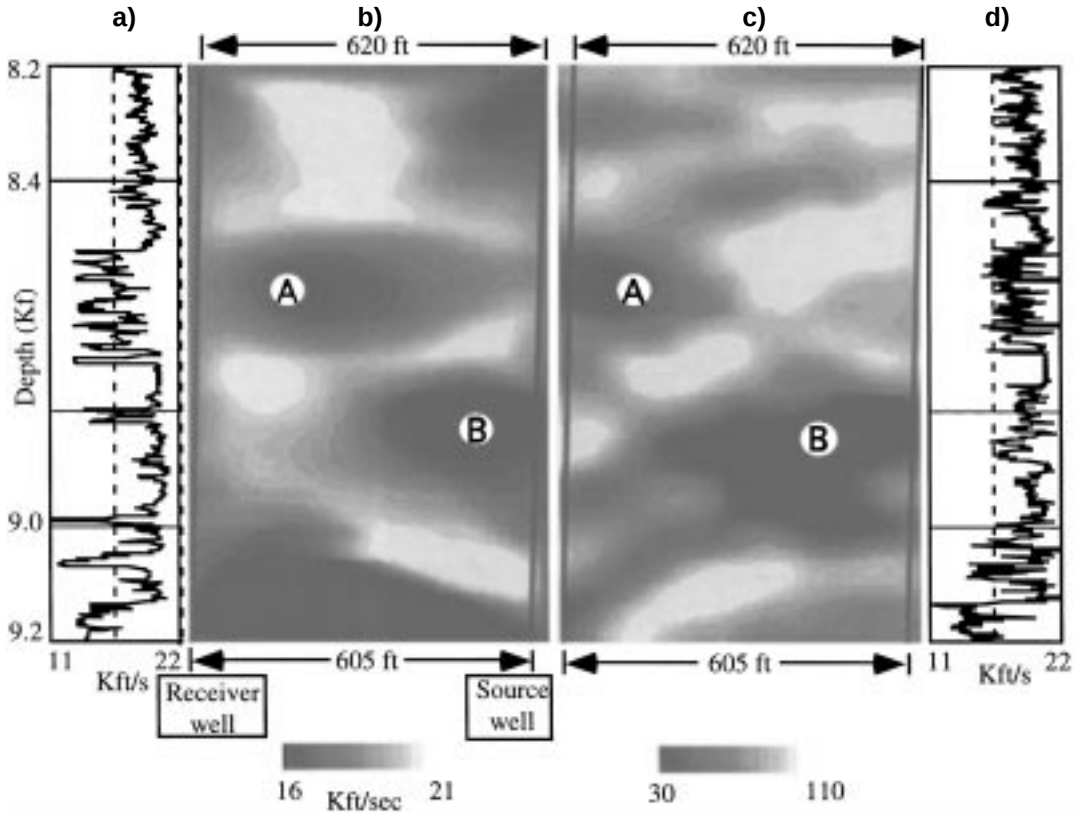

FIG. 14. The attenuation and velocity tomography for the west Texas survey. (a) Sonic log velocity in receiver well; (b) Crosswell velocity; (c) Crosswell Q; (d) Sonic log velocity in source well. The geological structure in this area is complex. The main features are two low-velocity/low-Q zones indicated by "A" and "B", respectively. Area B is interpreted as a carbonate mound or reef. The sonic log in the source hole matches tomograms. But the one in the receiver hole does not show the low-velocity/low-Q- zone indicated by "B". Area B is pay zone. Sonic log at this zone may only measure the velocity for the near borehole flushed layer, not the formation velocity.

CONCLUSIONS

Frequency-dependent attenuation causes a change in the amplitude distribution of a wave's frequency spectra. For a constant Q-model and a Gaussian spectrum this change is simple: the difference in centroid frequency between the incident (input) and transmitted (output) waves is proportional to the integrated attenuation multiplied by a scaling factor. This fact results in a simple formula that can be used for attenuation tomography. Spectra other than Gaussian can be handled by changing the scale factor, or using Gaussian as a curve fit to them. Although the method is sensitive to small frequency changes, it is best on data with a broad frequency band. The crosswell geometry with a high-frequency downhole source provides a good opportunity for using this method. Field data tests in 1-D and 2-D geology show that the attenuation tomograms have a good correlation with lithology and the velocity tomogram. Further research is underway to adapt the technique to sonic log analysis.

ACKNOWLEDGMENTS

A velocity inversion program originally written by Dr. Feng Yin was modified for the attenuation tomography. Feng Yin also helped in developing this algorithm. This work is supported by DOE under DE-FG03-95ER14535.A000. We are also grateful to the sponsors of the Seismic Tomography Project (STP) at Stanford University for supporting this work, British Petroleum for use of the Devine data set, and Chevron Petroleum Technology Company for use of the reef data set. We would also like to thank the reviewers of this paper for their excellent suggestions.

REFERENCES

Best, A. I., McCann, C., and Sothcott, J., 1994, The relationships between the velocities, attenuations, and petrophysical properties of reservoir sedimentary rocks: Geophys. Prosp., **42**, 151–178.

Brzostowski, M., and McMechan, G., 1992, 3-D tomographic imaging of near-surface seismic velocity and attenuation: Geophysics, **57**, 396–403.

Chen, X., Quan, Y., and Harris, J. M., 1996, Seismogram synthesis for radially layered media using the generalized reflection/transmission coefficients method: Theory and applications to acoustic logging: Geophysics, **61**, 1150–1159.

Dines, K., and Kak, A., 1979, Ultrasonic attenuation tomography of soft tissues: Ultrasonic Imaging, **1**, No. 1, 16–33.

Hauge, P., 1981, Measurements of attenuation from vertical seismic profiles: Geophysics, **46**, 1548–1558.

Johnston, D. H., 1981, Attenuation: A state-of-art summary: Seismic Wave Attenuation, *in* Toksöz, M. N. and Johnston, D. H., Eds., Geophysics reprint series, No. 2: Soc. of Expl. Geophys.

Kjartansson, E., 1979, Constant Q-wave propagation and attenuation: J. Geophys. Res., **84**, 4137–4748.

Leggett, M., Goulty, N. R., and Kragh, J. E., 1992, Study of traveltime and amplitude time-lapse tomography using physical model data: Abstracts of 54th EAEG Meeting, 248–249.

Luco, J. E., and Apsel, R. J., 1983, On the Green's function for a layered half-space, Part I: Bull. Seis. Soc. Am., **73**, 909–929.

Marion, D. P., and Coudin, P., 1992, From ray to effective medium theories in stratified media: an experimental study: Ann. Internat. Mtg., Soc. Expl. Geophys., Expanded Abstracts, 1341–1243.

Narayana, P. A., and Ophir, J., 1983, A closed form for the measurement of attenuation in nonlinearly dispersive media: Ultrasonic Imaging, **5**, 17–21.
Parker, K., Lerner, R., and Waag, R., 1988, Comparison of techniques for *in vivo* attenuation measurements: IEEE Trans. on Biomedical engineering, **35**, No. 12, 1064–1067.
Youli, Q., Chen, X., and Harris, J., 1996, Elastic waves in radially symmetric media: 66th Ann. Internat. Mts., Soc. Expl. Geophys., Expanded Abstracts,
Ward, R. W., and Toksöz, M. N., 1971, Causes of regional variation of magnitude: SSA Bull. **61**, 649–670.
Zucca, J. J., Hutchings, L. J., and Kasameyer, P. W., 1994, Seismic velocity and attenuation structure of the Geysers geothermal field, California: Geothermics, **23**, 111–126.

APPENDIX

RELATIONSHIPS BETWEEN THE ATTENUATION COEFFICIENT AND THE FREQUENCY SHIFT

If the input amplitude spectrum, $S(f)$ is of Gaussian shape, i.e.,

$$S(f) = \exp\left[-\frac{(f - f_o)^2}{2\sigma_S^2}\right], \tag{A-1}$$

then, the centroid of $S(f)$ is f_o. Assume that the factor G in equation (1) does not depend on frequency. From equations (1) and (2), we can write the output amplitude spectrum as

$$\begin{aligned} R(f) &= GS(f)H(f) \\ &= G\exp\left[-\frac{(f - f_o)^2}{2\sigma_S^2} - f\int_{ray}\alpha_o\, d\ell\right] \\ &= G\exp\left[-\frac{f^2 - 2ff_R + f_R^2 + f_d}{2\sigma_S^2}\right] \\ &= A\exp\left[-\frac{(f - f_R)^2}{2\sigma_S^2}\right], \end{aligned} \tag{A-2}$$

where

$$f_R = \left(f_o - \sigma_S^2\int_{ray}\alpha_o\, d\ell\right), \tag{A-3}$$

$$f_d = 2f_o\sigma_S^2\int_{ray}\alpha_o\, d\ell - \left(\sigma_S^2\int_{ray}\alpha_o\, d\ell\right)^2, \tag{A-4}$$

and

$$A = G\exp\left[-\frac{f_d}{2\sigma_S^2}\right]. \tag{A-5}$$

It can be seen that f_R is the centroid of $R(f)$, and A is its amplitude.

If the spectrum $S(f)$ is of rectangular shape with a width of B, then

$$f_S = \int_0^B f\, df \Big/ \int_0^B df = B/2, \tag{A-6}$$

$$\begin{aligned} f_R &= \frac{\int_0^B fe^{-fa_oL}df}{\int_0^B e^{-fa_oL}df} \\ &= \frac{a_oL}{1 - e^{-a_oLB}}\left[\frac{1}{(a_oL)^2} - \frac{Be^{-a_oLB}}{a_oL}\left(\frac{1}{a_oLB} + 1\right)\right]. \end{aligned} \tag{A-7}$$

For simplicity, we write $\int_{ray}\alpha_o\, d\ell$ as α_oL for a homogeneous medium. If $\alpha_oLB \ll 1$, we have

$$\exp(-\alpha_oLB) \approx 1 - \alpha_oLB + \tfrac{1}{2}(\alpha_oLB)^2 - \tfrac{1}{6}(\alpha_oLB)^2 \tag{A-8}$$

and

$$f_R \approx \frac{B}{2} - \frac{B^2}{12}\alpha_oL = f_S - \frac{B^2}{12}\alpha_oL, \tag{A-9}$$

or write it as tomographic equation

$$\int_{ray}a_o\, d\ell \approx 12(f_S - f_R)/B^2. \tag{A-10}$$

Similarly, if $S(f)$ is a right triangle with a side of B and $\alpha_oLB \ll 1$, we get

$$f_S = \tfrac{1}{3}B, \tag{A-11}$$

$$f_R \approx \frac{B}{3} - \frac{B^2}{18}\alpha_oL = f_S - \frac{1}{18}\alpha_oL \tag{A-12}$$

and

$$\int_{ray}a_o\, d\ell \approx 18(f_S - f_R)/B^2. \tag{A-13}$$